



Citation for published version:

Mahmood, I, Martinez Hernandez, U & Dehghani-Saniij, AA 2020, 'Evaluation of Gait Transitional phases using Neuromechanical outputs and somatosensory inputs in an Overground walk', *Human Movement Science*, vol. 69, 102558. <https://doi.org/10.1016/j.humov.2019.102558>

DOI:

[10.1016/j.humov.2019.102558](https://doi.org/10.1016/j.humov.2019.102558)

Publication date:

2020

Document Version

Peer reviewed version

[Link to publication](#)

Publisher Rights

CC BY-NC-ND

University of Bath

Alternative formats

If you require this document in an alternative format, please contact:
openaccess@bath.ac.uk

General rights

Copyright and moral rights for the publications made accessible in the public portal are retained by the authors and/or other copyright owners and it is a condition of accessing publications that users recognise and abide by the legal requirements associated with these rights.

Take down policy

If you believe that this document breaches copyright please contact us providing details, and we will remove access to the work immediately and investigate your claim.

1 **Evaluation of Gait Transitional phases using Neuromechanical outputs and**
2 **somatosensory inputs in an Overground walk**

3
4 Imran Mahmood ^{a,1}, Uriel Martinez-Hernandez ^b, Abbas A. Dehghani-Sanij ^a

5
6 ^a Institute of Design, Robotics, and Optimisation, School of Mechanical Engineering
7 University of Leeds, Leeds, United Kingdom

8 ^b Department of Electronic and Electrical Engineering,
9 University of Bath, Bath, United Kingdom

10
11 **Submitting for Original Article**

12
13
14
15
16 **¹ Corresponding Author**

17 Imran Mahmood

18 School of Mechanical Engineering

19 The University of Leeds,

20 Leeds, LS2 9JT, United Kingdom

21 Email: mnim@leeds.ac.uk

22 Phone +44(0)7589658714
23
24
25
26
27
28
29
30
31

Abstract

In a bipedal walk, the human body experiences continuous changes in stability especially during weight loading and unloading transitions which are reported crucial to avoid fall. Prior stability assessment methods are unclear to quantify stabilities during these gait transitions due to methodological and/or measurement limitations. This study introduces Nyquist and Bode methods to quantify stability gait transitional stabilities using the neuromechanical output (CoP) and somatosensory input (GRF) responses. These methods are implemented for five different walking conditions grouped into walking speed and imitated rotational impairments. The trials were recorded with eleven healthy subjects using motion cameras and force platforms. The time rate of change in O/Is illustrated impulsive responses and modelled in the frequency domain. Nyquist and Bode stability methods are applied to quantify stability margins. Stability margins from outputs illustrated loading phases as stable and unloading phases as unstable in all walking conditions. There was a strong intralimb compensatory interaction ($p < 0.001$, Spearman correlation) found between opposite limbs. Overall, both walking groups illustrated a decrease ($p < 0.05$, Wilcoxon signed-rank test) in stability margins compared with normal/preferred speed walk. Further, stabilities quantified from outputs were found greater in magnitudes than the instability quantified from inputs illustrating the neuromotor balance control ability. These stability outcomes were also compared by applying extrapolated-CoM method. These methods of investigating gait dynamic stability are considered as having important implications for the assessment of ankle-foot impairments, rehabilitation effectiveness, and wearable orthoses.

Key words: Gait, transitional phases, dynamic stability, Nyquist and Bode, neuromotor

54

55

56

57

58

59

60

61

62

63

64

65

66

67

68

69 Research Highlights

- 70 • Gait dynamic stability evaluated during loading and unloading transitions
- 71
- 72 • Neuromotor output and inputs measured from CoP and CoM-acceleration signals
- 73
- 74 • Nyquist and Bode methods introduced to quantify gait transitional stabilities
- 75
- 76 • Eversion and inversion foot impairments illustrated a significant decrease in stability
- 77
- 78 • Overground walking speeds partially impacted on gait transitional stabilities
- 79

80

81

82

83

84

85

86

87

88

89

90

91

92

93

94

95

96

97

98

99

100

101

102 1. Introduction

103 Gait dynamic stability is important for independence while performing daily living
104 activities. Various stability assessment techniques are reported earlier mainly categorised into
105 clinical and laboratory-based methods (Neptune & Vistamehr, 2018). Clinically, walking
106 stabilities are assessed applying Berge balance, Time up and go tests in which questionnaires
107 are used or stopwatch measurements are made from patients. Laboratory-based methods
108 involve sophisticated equipment and are reported with precise quantification of gait dynamic
109 stabilities. Laboratory methods are further categorised into discrete point or continuous time
110 series stability evaluations of a gait cycle using related measurement signals. Laboratory
111 methods are not yet being applied in clinical environments due to diversified outcomes and
112 multiple biomechanical signals being used. Further, the stability evaluation criteria in these
113 methods are based on a comparison between testing and control subjects to define a gait being
114 stable or unstable.

115 Considering methodological choices, firstly, the discrete events stability evaluations include
116 lower limb joints peak angles and moments (Soares, de Castro, Mendes, & Machado, 2014),
117 spatiotemporal parameters (step width, step length), or extrapolated center-of-mass (XCoM)
118 difference from base-of-support (BoS) (Hof, 2008; Sivakumaran, Schinkel-Ivy, Masani, &
119 Mansfield, 2018). In the second category, stability evaluations involve continuous time series
120 bulk data of measurement waveforms, these include, Lyapunov exponent, Floquet multiplier,
121 (Ihlen et al., 2012; Kang & Dingwell, 2009) and intraclass correlation methods (Rabuffetti et
122 al., 2011). These methods were used to quantify gait stabilities as a unit-less factor which was
123 assumed consistent over the entire stride. Both these discrete and continuous time series
124 methods are being indistinct to evaluate gait transitional phases i.e. loading and unloading
125 phases which are reported critical considering gait dynamic stabilities (Bizovska et al., 2014;
126 Svoboda et al., 2017). The loading and unloading phases include ~30% of stance from heel
127 contact and towards toe-off events respectively, also known as double limb support time in a
128 gait cycle. During these transitions, body weight is transferred from one limb to others
129 (Bizovska et al., 2014), neuromotor programs is modulated (Rabuffetti et al., 2011), and
130 muscles activate to maximum level to provide acceleration to trailing limb and decelerate to
131 the leading limb (La Scaleia, Ivanenko, Zelik, & Lacquaniti, 2014). Despite these vital
132 biological transformations taking place during these phases, the gait dynamic stabilities have
133 been remained unquantified during these gait phases.

134 Considering measurement signals, prior methods used multiple variables to evaluate gait
135 stabilities. For example, most widely used extrapolated-CoM (XCoM) method attempt to
136 quantify BoS from different foot positions, these include, foot centre of pressure (CoP)
137 trajectory, toe marker, or heel marker positions. This method quantifies margins of stability
138 (MoS) as XCoM maximum sways from BoS at HC and TO events and assumes double limb
139 support time zero (Hof, 2008). Another most reliable method 'Lyapunov exponent' is reported
140 to use multiple variables e.g. markers positions data from either trunk, pelvis, lower limb
141 segments, joints, EMGs or their higher order derivatives to evaluate dynamic stability. A few
142 studies are also reported to have criteria of at least five variables needed in the Lyapunov
143 exponent method to be precise (Kang & Dingwell, 2009). In comparison, the neuromotor
144 balance control theory states that lower limb muscles activate in response to CoM positions or
145 acceleration (Allen & Ting, 2016; Graham, Carty, Lloyd, & Barrett, 2017) and CoP gives
146 measure of resultant neuromotor balance control (Lugade & Kaufman, 2014), however, CoP is

147 independent to that of CoM (Winter, 2009). Despite the use of body's CoP and CoM being
148 widely reported in relation to stability evaluation, their application for gait transitional phases
149 stability evaluation has been remained uninvestigated due to methodological limitations.

150 More recent studies have introduced Nyquist and Bode (N&B) methods to quantify gait
151 dynamics stabilities related to knee deficiencies (Ardestani, ZhenXian, Noori, Moazen, & Jin,
152 2019; Morgan, Zheng, Bush, & Noehren, 2016) and postural perturbations (Hur, Duiser,
153 Salapaka, & Hsiao-Wecksler, 2010). These are control engineering stability analysis
154 techniques with the capability of evaluating transient and steady-state stabilities. Earlier, these
155 methods were widely used for design and control in medical robots, however, their application
156 in gait stability evaluations is relatively new. In this study, we have applied these methods
157 using resultant ground reaction forces (GRF) biomechanical signals such that the tail of GRF
158 vector presents CoP (output) and head of GRF vector presents CoM-acceleration (input)
159 responses by the neuromotor (Appendix Fig. A1). These methods are implemented here
160 specifically for stability evaluations during gait transitional phases.

161 **2. Methods**

162 *2.1. Participants*

163 A total of eleven healthy subjects participated in this study (age 30 ± 1 yr, weight 74 ± 3 kg,
164 and height 1.72 ± 2.5 m) after confirming no prior anatomical or neuromuscular impairments.
165 Each subject signed an informed consent form which was approved by the institutional ethical
166 review board at the University of Leeds.

167 *2.2. Experimental Protocol*

168 Two different walking conditions i.e. preferred walking speeds and rotational impairments
169 are simulated in this study to evaluate gait transitional stabilities. Following prior studies
170 (Rabiei, Eslami, & Movaghar, 2016; Soares et al., 2014), the rotational foot impairments were
171 imitated using self-designed wedge-shaped foot insoles (Fig. A3). The insoles were designed
172 in pairs using Styrofoam sheet (high density, thickness 1inch, compressive strength 690kPa)
173 and wedged to $\pm 10^\circ$ using a hot wire cutter. The Styrofoam material preserves the loading
174 impacts compared to commercially available soft insoles and helps in imitating eversion and
175 inversion foot deficiencies. In this study, these foot conditions were imitated to a moderate
176 range i.e. -10° laterally inclined insole for inverted/supinated foot and $+10^\circ$ medially inclined
177 insole for the everted/pronated foot. Each insole was further cut into two parts i.e. hindfoot and
178 forefoot to allow forefoot flexible motion during the push-off phase. Both parts were joined
179 together using gaffer tape. These insoles were made portable to perform dynamic activities and
180 worn by each participant using Velcro straps.

181 *2.3. Data Collection*

182 The trials were conducted in motion capture lab using 12 infrared cameras (Oqus cameras,
183 400 Hz), two force platforms (AMTI BP400600-2000, 1 kHz), and 26 reflective markers were
184 attached to each subject at lower limbs as illustrated in Fig. A1. The placement of the markers
185 was made following Visual-3D help document (C-Motion_Markers, 2019) as illustrated in Fig.
186 A2. There are two distinct force plates mounted on the lab floor in the pathway. The subjects
187 were instructed to adjust their steps to ensure each foot was positioned at a separate force plate.
188 After getting familiar, the experiments were recorded using Qualisys software. Each force plate

189 measures three-dimensional (3D) ground reaction forces (GRFs) and two-dimensional (2D)
190 centre of pressure (CoP) position trajectories. The recorded data from each foot was used for
191 further analysis. Each subject performed five trials for each of the five walking conditions.
192 These five walking conditions were further grouped into walking speed (slow, normal and fast)
193 and rotational foot impairments (everted and inverted foot). A self-selected normal speed walk
194 was considered as a reference in both groups. The sequence in which trials were recorded
195 included slow, normal, and fast speed trials at first and thereafter imitated inverted and everted
196 foot walking conditions were performed at a self-selected preferred walking speed. While
197 simulating rotational foot impairments, each subject was asked to get familiar by walking with
198 wedged insoles in both feet, and after feeling comfortable, the trials were recorded. The trials
199 were recorded on an 8m walking track. During each trial, the data from the limb movements
200 were recorded in terms of 3D marker coordinates, 3D GRFs, and 2D CoP-position. Markers
201 coordinates were used to compute ankle-foot angles and margin-of-stability (MoS). The GRFs
202 and CoP position data were used to evaluate stability margins in anterior-posterior and medial-
203 lateral directions.

204 *2.4. Data Processing*

205 The rotational ankle-foot angles for simulated walking conditions were computed in the
206 Visual-3D motion analysis software (Fig. A4) following the procedure defined in the
207 software's help document (C-Motion_Angles, 2019). Firstly, lower-limb markers position data
208 was exported to Visual-3D software as C3D files. Each C3D file includes 26 markers (x, y, z)
209 coordinates those were attached to foot, ankle and shank segments. Secondly, this data was
210 used to construct the body's anatomical model, and finally, a built-in command used to
211 compute rotation of foot w.r.t shank reference. The rotation of foot w.r.t shank measures ankle
212 joint angles along (x, y, z) directions. The rotational angles present the rotation of ankle-foot
213 along the anterior-posterior axis of the ankle-foot joint. An outward ankle-foot rotation is called
214 inversion and an inward rotation is called eversion. The outcomes from everted/inverted foot
215 simulations abnormalities (using $\pm 10^\circ$ wedged insoles) were further confirmed by evaluating
216 ankle-foot rotational angles experimentally in Visual-3D. Fig. 4 illustrates the trajectories
217 (mean \pm Std.) for the normal, everted and inverted foot conditions. A maximum difference of
218 everted and inverted foot trajectories was computed w.r.t to the normal foot trajectory. These
219 differences in rotational angles were found as $6.66^\circ(\pm 2.67)$ for the everted foot and
220 $6.77^\circ(\pm 2.49)$ for an inverted foot condition. These experimentally obtained rotational angles
221 are in approximation to the wedged angles of wearable insoles. These ranges imitate moderate
222 range rotational impairments and are consistent with a previous study (Rabiei et al., 2016). The
223 ground reaction force (GRF) and CoP raw data were exported directly to MATLAB-2017a.
224 The anterior-posterior and medial-lateral components of both of these two signals were
225 processed further. For each of the individual subjects, the GRF (Newton) data recorded during
226 each trial was normalised by the respective subject's body mass (kg) to obtain CoM-
227 acceleration (i.e. GRF/mass). For each of the measured signals, both the amplitude and
228 respective time axes information was used for further processing. The time rate of change of
229 CoP and CoM-acceleration were computed. In each trial, both amplitude and time axes were
230 recorded for the whole stance phase which was further analysed by diving stance into
231 subphases (i.e. loading and unloading). These sub-phases also present initial and ending double
232 limb support phases of a gait cycle (Bizovska et al., 2014). The input data set for each of the
233 measured signals consist of (100 samples \times 55 trials). Equations (1-3) were applied to the rows

234 (i.e. samples in each column) such that two consecutive samples were used to compute mean
 235 CoP-velocity and RMS CoM-oscillations for respective input signals. For each trial, at first,
 236 equation (1) was applied to compute actual CoP-velocity and thereafter equation (2) was
 237 applied to compute mean values of the actual CoP-velocities following (Bizovska et al., 2014;
 238 ImageJ-macros, 2019; Mei et al., 2013). The averaging of actual CoP-velocity applying Eq. 2
 239 helps to smoothen the noise as also illustrated in Fig. 1(a). Similarly, equations (1) and (3) were
 240 used to compute the rate of change in CoM-acceleration and RMS CoM-oscillations following
 241 (Cattaneo et al., 2014; Rabuffetti et al., 2011).

$$242 \quad V_{COP_actual} = \frac{d_{xi}}{d_{ti}} = \frac{|y_{i+1}-y_i|}{|t_{i+1}-t_i|} \quad (1)$$

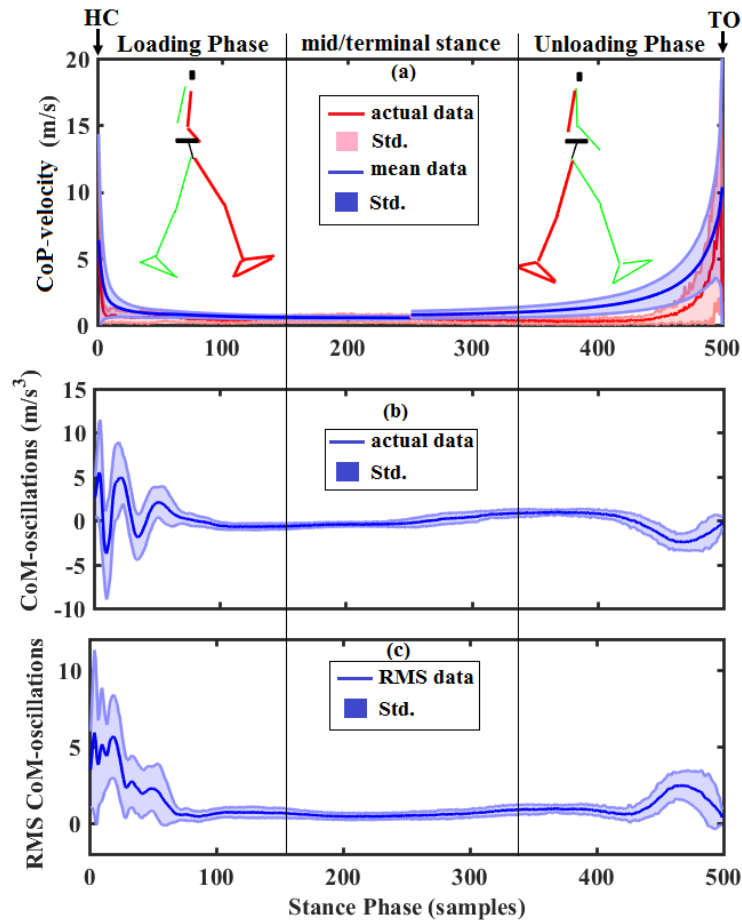
$$243 \quad V_{COP_average} = \frac{d_{xi}+d_{x_sum}}{d_{ti}+d_{t_sum}} \quad (2)$$

244 Where ' d_{xi} ' and ' d_{ti} ' are the differences between two consecutive samples measuring CoP
 245 positions i.e. y_i, y_{i+1} and time samples i.e. t_i, t_{i+1} . Similarly, ' d_{x_sum} ' and ' d_{t_sum} ' present
 246 the sum of previous differences and current samples difference.

$$247 \quad a_{\dot{CoM}} = \sqrt{(\dot{a}_1^2 + \dot{a}_2^2)/2} \quad (3)$$

248 Where ' $a_{\dot{CoM}}$ ' presents RMS value of CoM-oscillation, ' \dot{a}_1 ' and ' \dot{a}_2 ' are the rate-of-change of
 249 CoM-acceleration and present two consecutive samples of a waveform.

250 During the loading phases, both signals (mean CoP-velocity and RMS CoM-oscillations)
 251 showed the instant rise and thereafter exponential decay in magnitudes. Oppositely during
 252 respective unloading phases, an exponential rise and thereafter an instant decay was observed
 253 in the measurement signals as illustrated in Fig.1. Following engineering control theory, a
 254 linear dynamic system that illustrates the aforementioned signal characteristics is considered
 255 as an output response to the unit impulse input. That unit input assumption helps in identifying
 256 the best-fit model by applying reverse engineering i.e. model identification approach as
 257 reported previously (Anderson et al., 2009; Morgan et al., 2016). These impulsive responses
 258 were windowed such that initial 30% of stance from HC presented as loading phase and last
 259 30% towards toe-off presented as unloading phase (Bizovska et al., 2014). The mean CoP-
 260 velocity impulses were filtered applying first-order Butterworth at 30Hz following (van der
 261 Linden, van der Linden, Hendricks, van Engelen, & Geurts, 2010) and RMS CoM-oscillations
 262 were filtered using second-order Butterworth at 10Hz (Sivakumaran et al., 2018).



263

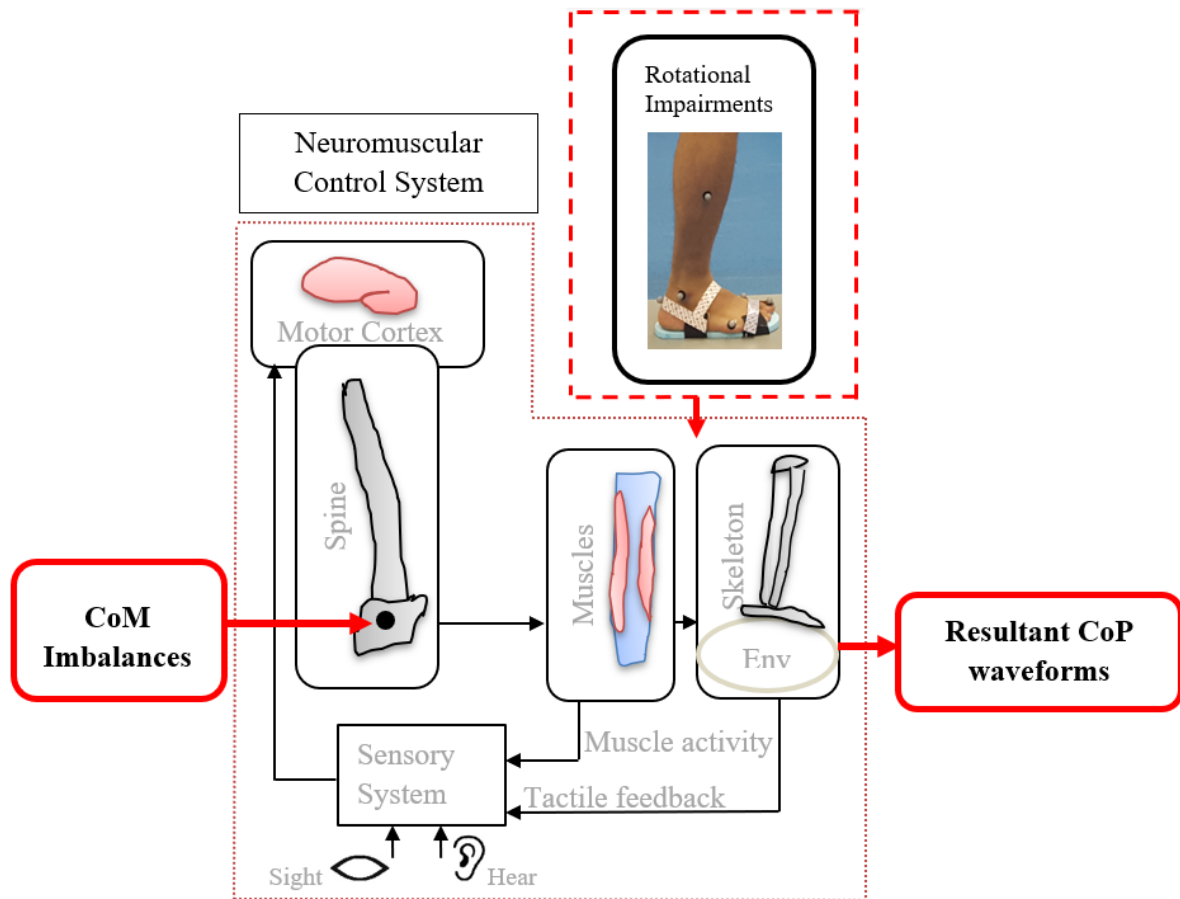
264 Fig. 1. Impulsive waveforms during gait transitions. The time rate of change in CoP and
 265 CoM-acceleration illustrated during loading and unloading phases for normal speed trials in
 266 the anterior-posterior direction. For each of the actual, mean, and RMS plots of respective
 267 signals, each data set present $\text{mean} \pm \text{Std.}$ for 55 trials (i.e. 11 subjects \times 5 trials). (a) CoP-
 268 velocity actual and mean data, (b) CoM-oscillations actual data, (c) Root-mean-square (RMS)
 269 values of CoM-oscillations.

270 Following neuromotor balance control, in this study, the CoP and CoM-oscillations are
 271 modelled as output and input responses respectively as shown in Fig. 2. It is widely reported
 272 earlier that any change in the body's CoM-acceleration acts as a feedback to reweight
 273 neuromotor control to activate lower limb muscles (Allen & Ting, 2016; Blum, Lamotte
 274 D'Incamps, Zytnicki, & Ting, 2017; La Scaleia et al., 2014). Similarly, the CoP is reported as
 275 a measure of neuromuscular control towards posture and gait (Lugade & Kaufman, 2014;
 276 Portela, Rodrigues, & de Sá Ferreira, 2014; Winter, 2009), however, the CoP trajectory is
 277 independent to the CoM. Following these well-known facts, we have modelled and analysed
 278 both signals independently. Also, prior studies analysed CoP (Bizovska et al., 2014;
 279 DiDomenico, McGorry, & Banks, 2013; Lugade & Kaufman, 2014) and CoM-acceleration
 280 (Cattaneo et al., 2014; Lencioni et al., 2014; Rabuffetti et al., 2011) signals independently while
 281 evaluating gait dynamic stability. A detailed neuromotor balance control loop is constructed in
 282 Fig. 2 with all constituent components. Considering neuromotor feedbacks, CoM-oscillations
 283 are reported as major somatosensory feedback that counts almost 70% along with vision and
 284 hearing those contribute 30% in overall (Bekkers et al., 2014). Summarising, CoP reflects
 285 changes in neuromotor independently in Fig. 2 and CoM-oscillations acts as a biomechanical

286 [trigger to whom neuromotor respond](#). One requirement of applying N&B analyses techniques
287 is the linear time-invariant models of the measuring system. The resultant waveforms (i.e. mean
288 CoP-velocity and RMS CoM-oscillations) illustrated artefacts due to repeated trials performed
289 with multiple subjects which included differences in anthropological data, markers adjustments
290 and foot insoles placements. These artefacts induce non-linearity in the data, hence, cleaned by
291 applying principal component analysis (PCA) following earlier studies (Anderson et al., 2009;
292 Sklavos, Porrill, Kaneko, & Dean, 2005; Tan & Hammond, 2007). [The PCA transform the](#)
293 [output data as a linear combination of involved variables, implemented here for individual](#)
294 [walking conditions and transitional phases following \(Maslivec et al., 2018\).](#)

295 The time-series waveforms for both loading and unloading phases were cleaned from
296 artefacts by applying PCA. The methodological choice of PCA is adapted from earlier studies
297 (Anderson et al., 2009; Maslivec et al., 2018; Robbins, Astephen Wilson, Rutherford, &
298 Hubley-Kozey, 2013). Also, the Inspect 3D software (Inspect3D, 2018) was used for repeated
299 measure data artefacts removal, however, we implemented PCA using MATLAB. The input
300 variables are mean CoP-velocity and RMS CoM-oscillations. Each of the repeatedly measured
301 variables consists of time-series waveforms data (input matrix:100×55), where 100 presents
302 samples per trial and 55 presents the total number of trials (11 subjects×5 trials). PCA converts
303 measured waveforms into various time dimensions also known as orthogonal signals (Cohen,
304 2014). The variance in these repeatedly measured input waveforms is described along each
305 time dimension also known as principal components (orthogonalized signals). General criteria
306 reported earlier is that the PCs should be used which explained at least 80% of the variability
307 (Robbins et al., 2013).

308 In this study, principal components (PCs) that explain maximum variance (>90%) are used
309 for reconstruction. For each variable, the output waveforms were reconstructed using $X=ZU^t$
310 (Z: score matrix, U: coefficient matrix, X: output matrix). The PCA performed here also helps
311 to approximate the linear behaviour of time-series data that follows prior studies with similar
312 changing period signal characteristics (Anderson et al., 2009; Downes et al., 2012; Sklavos et
313 al., 2005). A low dimensionality in our data indicates a low-order linear model for the
314 underlying system and any non-linearities are likely to be small. Hence, the least-square linear
315 regression models are identified as best-fit to the measured waveforms. The mean of each
316 subject's reconstructed waveforms (trials) was used in subsequent analysis.



317

318 Fig. 2. Neuromotor balance control illustrated using resultant biomechanical signals. The
 319 CoM imbalances quantified as CoM-oscillations (rate-of-change in CoM-acceleration) acts as
 320 somatosensory input that acts as a feedback to reweight muscles activity at the onset of the
 321 perturbations. The centre-of-pressure (CoP) measures resultant neuromuscular response
 322 towards posture and gait, independent to the centre-of-mass (CoM).

323 2.5. Frequency domain Transfer Functions (TFs)

324 The loading and unloading phases reconstructed waveforms were modelled using least
 325 square linear regression technique. A sum of exponent models was found the best fit (R^2 :
 326 $99\pm 0.5\%$) for CoP-velocity and a sum of sinusoidal functions was found the best fit (R^2 :
 327 $99\pm 0.5\%$) for CoM-oscillations. These time-domain models were converted to frequency
 328 domain applying Laplace transformation in MATLAB-2017a following (Morgan et al., 2016)
 329 and resultant models are named as transfer functions (TF). A transfer function is the ratio of
 330 Laplace of output to input polynomials. The roots of numerator polynomial present zeros of a
 331 TF and roots of denominator polynomial present poles of a TF. If the poles lie on the left half
 332 of the s-plane the system is defined as stable, otherwise unstable.

333 2.6. Nyquist and Bode Stability Criteria

334 Nyquist and Bode methods are implemented by assuming linear time-invariant models as
 335 illustrated by low dimensionality (PCA) in the input waveforms for both mean CoP-velocity
 336 and RMS CoM-oscillations. Both of these two signals quantify resultant effects of whole limb
 337 motions, hence, non-linearities in CoM-oscillations caused by mass-inertia changes around the
 338 individual joints (ankle, knee and hip) are likely to be small. These open-loop TFs modelled

339 from CoP-velocity and CoM-oscillations were excited by unit impulse input perturbations
 340 (Morgan et al., 2016) and stability margins were quantified following Nyquist and Bode
 341 stability criteria (Bavafa-Toosi, 2017). The Nyquist plot presents a TF/model in a polar plot in
 342 which the point $(-1, 0j)$ is used to define critical stability. The difference of a system's gain and
 343 phase plots from this critical point is used to quantify stability as gain margin (GM) and phase
 344 margin (PM) (Fig. A5). The gain margin (decibel/dB) presents the magnitude of a system's
 345 gain at a frequency where the corresponding phase plot cuts $\pm 180^\circ \pm 2k\pi$ axes (Bavafa-Toosi,
 346 2017). Similarly, the phase margin (degrees) presents the magnitude of a phase at a frequency
 347 where the corresponding gain plot cuts the 0dB axis. In control theory, a GM measures
 348 robustness of a system and a PM measures the stability of a dynamic system. These margins
 349 present the difference from an unstable region if a system is stable, conversely these present
 350 the distance from a stable region if a system is unstable. A system might have multiple gain
 351 and phase margins, however, the smallest of them is considered critical as it is closest to
 352 instability region if presented for a stable system, and vice-versa (Bavafa-Toosi, 2017).

353 *2.7 Extrapolated-CoM difference from BoS*

354 For comparing between gait events and phases stabilities, the discrete events based MoS(s)
 355 were also evaluated by computing extrapolated-CoM (XCoM) and BoS following the methods
 356 used by (Lugade, Lin, & Chou, 2011; Sivakumaran et al., 2018). The XCoM difference from
 357 BoS boundary (CoP position) was computed at heel contact (HC) and toe-off (TO) events in
 358 both anterior-posterior and medial-lateral directions. The MoS(s) at HC presents the starting
 359 point of a loading phase and at TO event presents ending point of an unloading phase. A
 360 decrease in MoS(s) gives an indication of poor balance control, however, in some cases, an
 361 increase in XCoM movement w.r.t BoS at toe-off also indicates poor balance control (Lugade
 362 et al., 2011). In this study, a decrease in MoS(s) at toe-off event is considered as an indication
 363 of poor balance control compared with control subjects trials at normal speed.

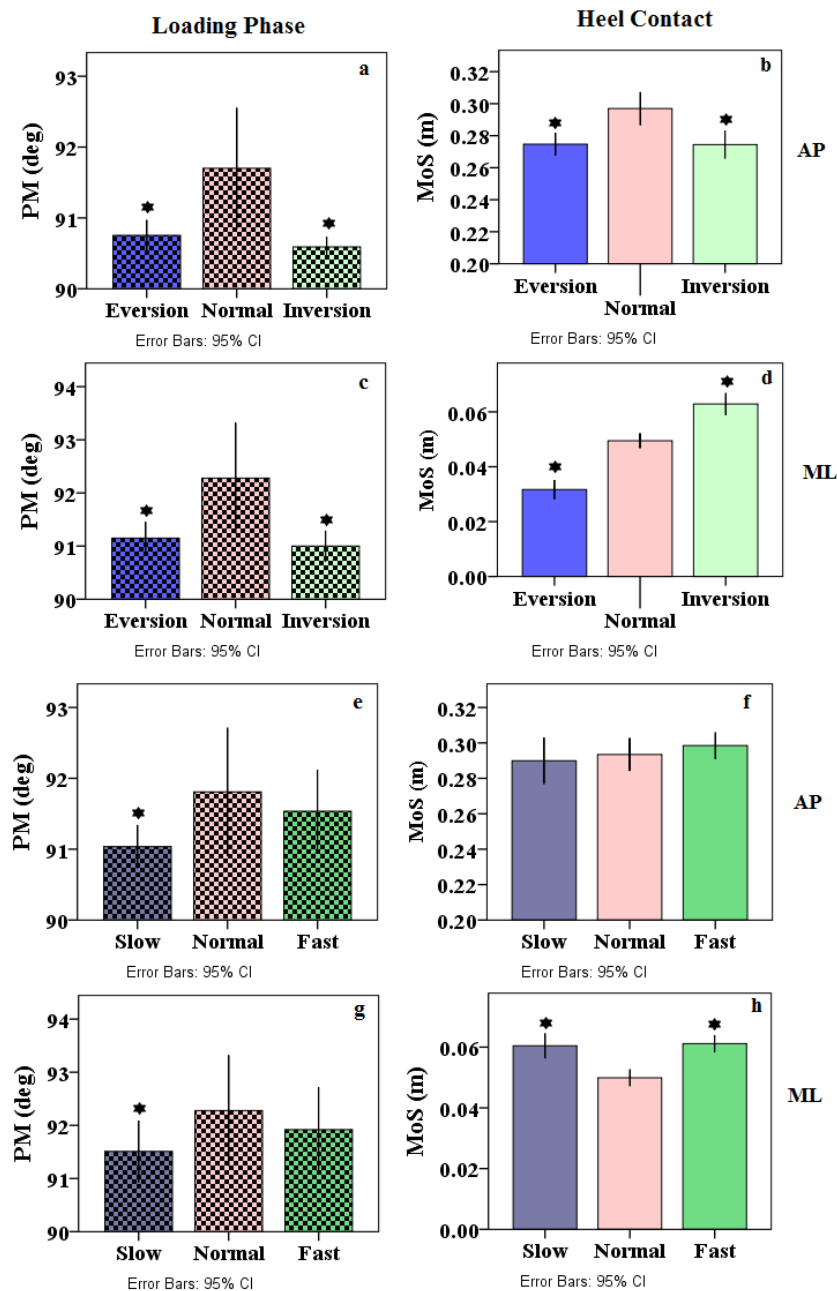
364 *2.8 Statistical Comparison*

365 After analysing the modelled TFs, the stability outcomes i.e. GM, PM, and MoS are tested
 366 for the normality applying Shapiro-Wilk test. Observing non-normality in the data ($p < 0.05$),
 367 the Wilcoxon signed-rank test was applied in SPSS (version 23, Chicago, IL, USA) to compare
 368 stability outcomes between simulated walking conditions and a normal walk. A parameter was
 369 considered statistically significant if $p < 0.05$. Also, both mean CoP-velocity and RMS CoM-
 370 oscillation waveforms illustrated non-normal distribution. Hence, the Spearman's correlations
 371 were evaluated between intralimb mean CoP-velocities (O/P), and between mean CoP-velocity
 372 (O/P) and RMS CoM-oscillations (I/P).

373 **3. Results**

374 The best fit models to CoP-velocity (O/P) waveforms illustrated stable responses in loading
 375 phases and unstable responses during unloading phases. Considering rotational impairments,
 376 the stability (PM) decreased ($p < 0.05$) in both everted and inverted foot walks during loading
 377 phases (Fig. 3a) and instability (GM, PM) decreased ($p < 0.05$) in an inverted foot alone during
 378 respective unloading phases (Fig. 4a, Table A1) in anterior-posterior (AP) direction. In medial-
 379 lateral (ML) direction, both rotational impairments showed a decrease ($p < 0.05$) in stability
 380 (Fig. 3c), however, there was no significant difference found during unloading phases (Fig.
 381 4c). Considering walking speed group, the stability (PM) decreased ($p < 0.05$) at slow speed in

382 loading phase (Fig. 3e and 3g) and instability (GM, PM) decreased ($p < 0.05$) at fast speed
 383 during unloading phases (Fig. 4e and 4g).

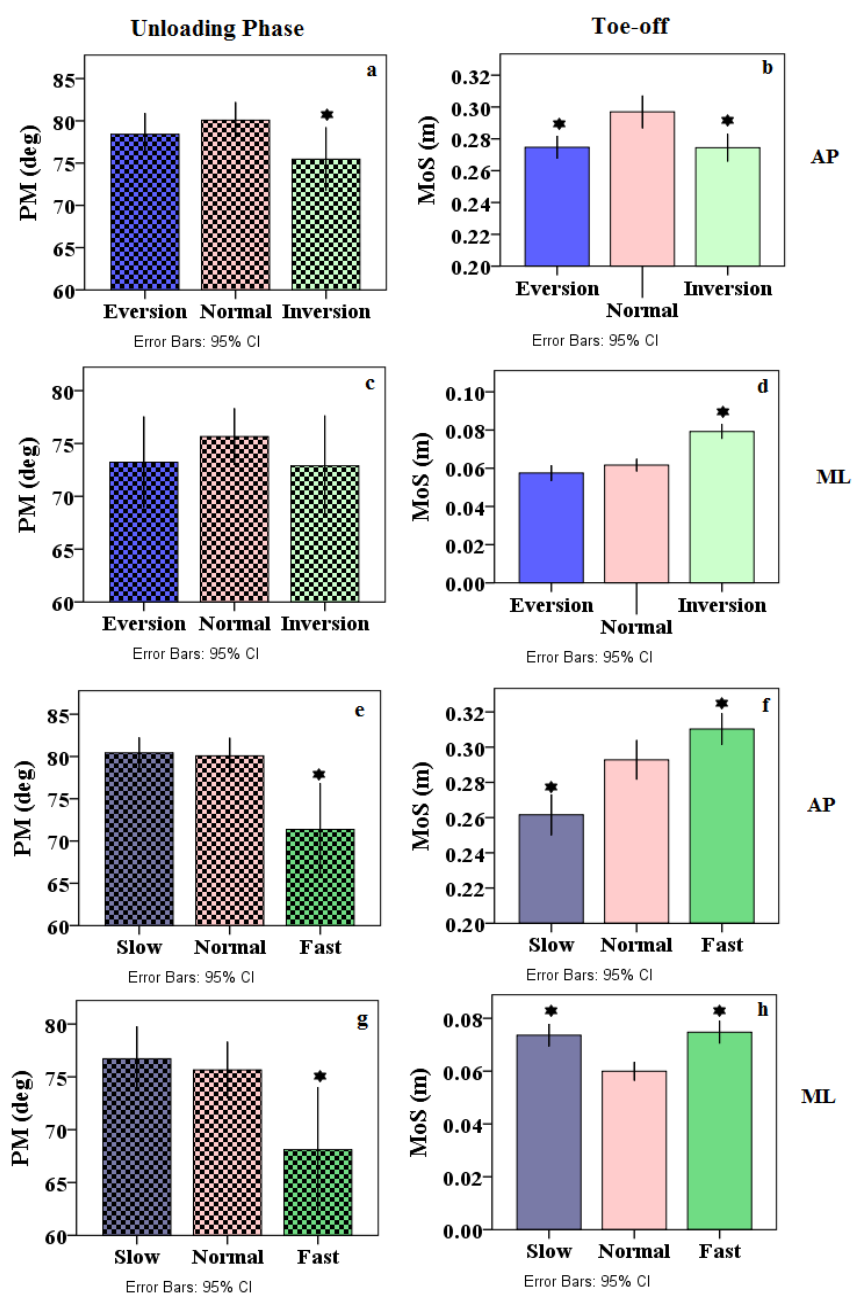


384

385 Fig. 3. Stability margins comparison during loading phases applying N&B methods (left) and
 386 extrapolated-CoM method (right). (a-d) rotational impairments in anterior-posterior (AP) and
 387 medial-lateral (ML) directions, (e-h) walking speed group in AP and ML directions, * shows
 388 significant ($p < 0.05$) difference.

389 Considering rotational impairments, in AP direction, both eversion and inversion conditions
 390 showed a decrease ($p < 0.05$) in MoS(s) at HC (Fig. 3b, Table A1) and TO (Fig. 4b, Table A1).
 391 In ML direction, an inverted foot walk illustrated an increase in MoS(s) at both HC (Fig. 3d)
 392 and TO (Fig. 4d) events. An everted foot showed a decrease in MoS only at HC (Fig. 3d). The
 393 MoS(s) quantified from the extrapolated-CoM method at HC showed no significant difference
 394 in walking speeds in AP direction (Fig. 3f), however, increased in ML direction (Fig. 3h). At

395 TO event, MoS decreased ($p<0.05$) at slow speed and increased at fast speed in AP direction
 396 compared to a normal walk (Fig. 4f). Both slow and fast speed walks illustrated increased
 397 MoS(s) in ML direction (Fig. 4h).

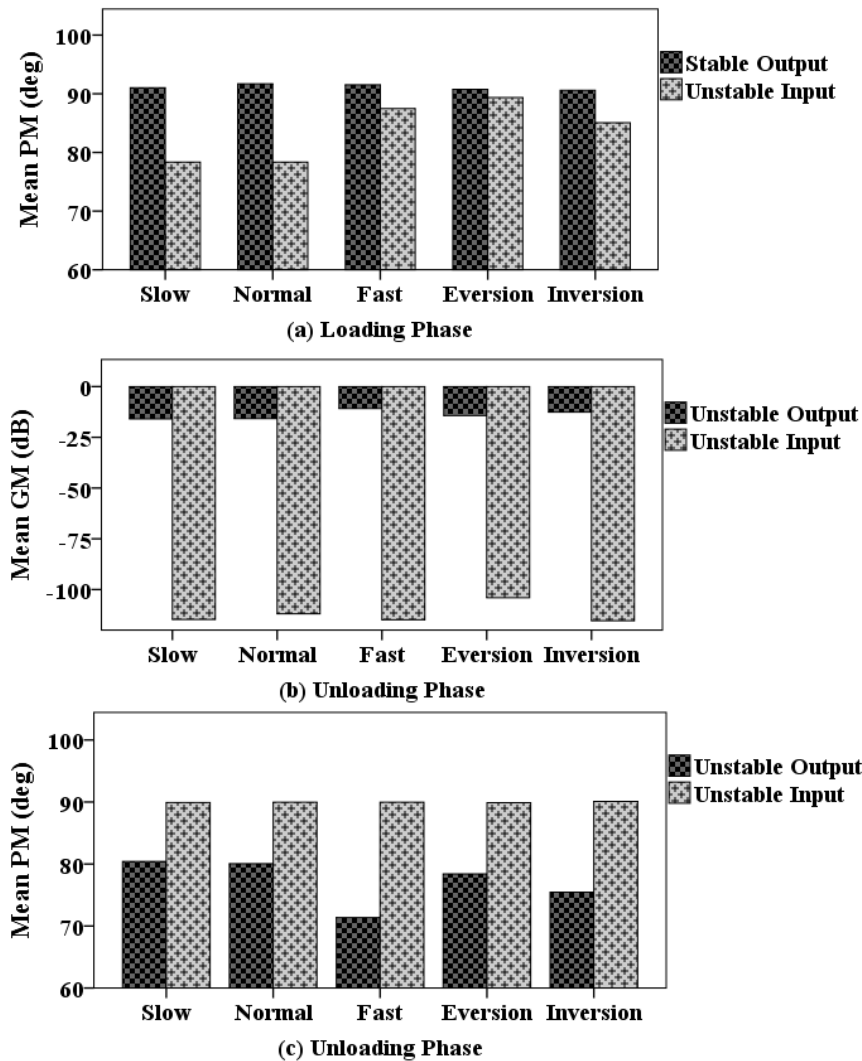


398

399 Fig. 4. Instability margins comparison during unloading phases applying N&B methods (left)
 400 and extrapolated-CoM method (right). (a-d) rotational impairments in anterior-posterior (AP)
 401 and medial-lateral (ML) directions, (e-h) walking speed group in AP and ML directions, *
 402 shows significant ($p<0.05$) difference.

403 Comparatively, the best-fit CoM-oscillations (I/P) models illustrated unstable responses
 404 during both loading and unloading phases (Table A2) in AP direction. In a rotational group,
 405 the instability (PM) was increased in an everted foot walk during loading and in an inverted
 406 foot walk during the unloading phase. During loading phases, a walk at fast speed showed an
 407 increase ($p<0.05$) in instability in terms of PMs, and during unloading, a slow speed walk

408 decreased ($p < 0.05$) in instability. However, the instability quantified by GMs at fast speed
 409 decreased ($p < 0.05$) during loading and increased in unloading phases. Stability margins
 410 quantified from I/Ps were compared with one from O/Ps for each of the walking conditions as
 411 illustrated in Fig. 5.



412

413 Fig 5. Comparison of neuromotor outputs and inputs. Stability margins quantified from the
 414 neuromotor output (CoP-velocity) and input (CoM-oscillation) responses in the anterior-
 415 posterior direction. The input instability is greater than outputs in all walking conditions.

416 An intralimb interaction between loading and unloading phases CoP-velocities (Table 1)
 417 showed strong negative correlations between them with $p < 0.001$ in respective walking
 418 conditions. However, there was no correlation found between CoP-velocity and CoM-
 419 oscillations during both loading and unloading phases.

420 **Table 1. Spearman's correlation between opposite limbs loading and unloading phases.**

Walking Conditions	Normal (p-value)	Eversion* (p-value)	Inversion* (p-value)	Slow (p-value)	Fast (p-value)
Anterior-posterior	-0.809 (0.001)	-0.834 (0.001)	-0.779 (0.001)	-0.864 (0.001)	-0.778 (0.001)

Medial-lateral	-0.842 (0.001)	-0.812 (0.001)	-0.791 (0.001)	-0.777 (0.001)	-0.772 (0.001)
-----------------------	-------------------	-------------------	-------------------	-------------------	-------------------

421 *Symmetric restrictions applied for both right and left foot.

422

423 **4. Discussion**

424 This study evaluates dynamic stability during gait transitional phases applying Nyquist and
 425 Bode (N&B) methods. Overall results illustrated significant differences in stability margins
 426 with the effect of self-selected walking speeds and rotational impairments. In this study,
 427 walking stabilities are evaluated using resultant neuromechanical O/I signals i.e. CoP and
 428 CoM-acceleration that provide redundancy in measurements compared with multiple signals
 429 being used earlier. Further, N&B methods used a distinct cut-off (0dB, $\pm 180^\circ \pm 2k\pi$) to define
 430 and quantify stable or unstable gait phases independent to comparing with control subjects.
 431 This implies that the stability definitions are standardized rather being dependent on fluctuating
 432 references. The phase margins quantified applying N&B methods are also compared with
 433 extrapolated-CoM method, however, the former evaluates stabilities within gait phases
 434 (loading and unloading) and the later evaluates discrete gait events (HC, TO) which present
 435 start and endpoints of respective phases.

436 Studies regarding neuromotor control reported the independence of CoP signals from CoM
 437 (Winter, 2009). Our results confirmed this statistically and illustrated poor correlation
 438 (Spearman's correlations) between these two signals. This biological fact helps to analyse both
 439 signals independently. The methodological steps defined here for CoP or CoM-acceleration
 440 based stability analysis are adopted from literature with waveforms having similar time-varying
 441 characteristics (Anderson et al., 2009; Downes et al., 2012). The most important one is the
 442 linear model identification for the plant. A plant model is identified from lower limb balance
 443 control signals i.e. CoP measures resultant neuromotor output and CoM-acceleration measures
 444 somatosensory feedback which counts almost 70% (Bekkers et al., 2014) of all neuromotor
 445 feedbacks. The time rate-of-change illustrated impulsive nature characteristics of measured O/I
 446 signals, that enable us to quantify the time and amplitude differences between normal and other
 447 simulated walking conditions. The PCA applied here to clean the O/I signals illustrated a low
 448 dimensionality that helps to approximate plant O/Is as linear regression models following
 449 (Anderson et al., 2009). Prior studies analyse CoP/CoM signals in the time domain and stability
 450 outcomes are reported for the whole gait cycle in terms of either range-of-motion (ROM)
 451 (Lugade & Kaufman, 2014) or the time constant and residual instability (Cattaneo et al., 2014;
 452 Rabuffetti et al., 2011). The methods define here quantify gait transitional phases i.e. weight
 453 loading and unloading gait sub-phases which are critical in muscles activation and hence in
 454 neuromotor balance control. In this study, a frequency domain analysis to the modelled signals
 455 provides a way to extract important balance control differentials (i.e time differences as PM
 456 and amplitude differences as GM) with standard set criteria.

457 The stability margins from neuromechanical O/P illustrated loading phases as stable and
 458 unloading phases as unstable. This is consistent with extrapolated-CoM method in which
 459 XCoM was reported within BoS at heel contact as a measure of stability and swayed outside
 460 the BoS at toe-off gave a measure of instability (Lugade et al., 2011). Further, our results
 461 illustrated a strongly negative correlation between opposite limb loading and unloading phases
 462 CoP-velocities (O/P). Both loading and unloading phases took place in parallel but out of

463 phase. This correlation illustrates that one limb during its loading phase (stable) is used to
464 compensate for the opposite limb's unloading phase (unstable) by an intralimb interaction. This
465 interaction is also reported earlier in elderly subjects which used their leading limb to
466 compensate the reduced push-off from trailing limb (Hernández, Silder, Heiderscheit, &
467 Thelen, 2009). However, there was no correlation found between rate dependant CoP and
468 CoM-acceleration waveforms which showed their independence consistent with findings
469 reported by Winter (Winter, 2009).

470 The results from rotational impairments showed a decrease in stability margins in loading
471 phases observed both in anterior-posterior and medial-lateral directions. That was due to the
472 reduced area during foot contact (HC) with the floor in these conditions (Öunpuu et al., 2013).
473 These findings were also determined to be consistent with event-based MoS(s) evaluations.
474 Overall, the inverted foot was found least stable in this group with decreased PM(s) both in AP
475 and ML directions. Previously, the inverted ankle sprain is described as the most sensitive
476 sports injury and has a chronic contribution towards gait instability (Hernández et al., 2009).

477 During respective unloading phases, our methods showed a decrease in inverted foot
478 instability in the forward direction (AP). That is consistent with outcomes reported in lateral
479 ankle sprains patients who were observed reluctantly to put bodyweight at the forefoot (Ihlen
480 et al., 2012). However, the MoS(s) applying extrapolated-CoM method showed a decrease in
481 MoS(s) at TO event (poor balance control) compared to a normal walk. In the medial-lateral
482 direction, N&B stability methods showed decreasing trends in instability for both inversion
483 and eversion, however, remained statistically insignificant whereas MoS illustrated an increase
484 in instability in the inverted foot. These contradictions between GMs and MoS(s) might be due
485 to the consideration of CoM along with CoP in MoS evaluations that increases/decreases the
486 sensitivity of measurements whereas N&B methods analysed CoP and CoM signals
487 independently as a neuromotor O/I. Our methods (N&B) illustrated that the rotational
488 impairments significantly affected gait transitional stabilities with a decrease in stabilities
489 during loading and decrease in instability during unloading phases.

490 The effect of walking speed on gait dynamic stability is reported earlier with inconsistent
491 outcomes e.g. slow walking speed is reported more stable in one study and negated in another
492 (Bruijn, van Dieën, Meijer, & Beek, 2009; Gigi et al., 2015). The stability margins quantified
493 here at self-selected walking speed showed that a normal/preferred speed walk was more stable
494 (PM) than a slow walk and had no difference with fast speed during the loading phase. This
495 finding is consistent with studies (Fan, Li, Han, Lv, & Zhang, 2016; Kavanagh, 2009) in which
496 a preferred walking speed showed the best compromise for frontal plane stability during single
497 limb support and smooth weight transfer during double limb support. A self-selected normal
498 walking speed is also reported to conserve the transformation energies (kinetic to potential and
499 vice versa) during gait transitions (Beyaert, Vasa, & Frykberg, 2015; Lu, Kuo, Chang, Lu, &
500 Hong, 2017). During respective unloading phases, a decrease in instability at fast speed walk
501 made its preference over slow and normal speed walks which did not illustrate any mutual
502 difference. This is consistent with findings from a prior study in which a fast speed walk is
503 reported with increased stability considering entire gait cycle waveforms applying local
504 dynamic stability method (Lu, Lu, Lin, Hsieh, & Chan, 2017). The extrapolated-CoM also
505 supported these findings with increased MoS(s) at fast speed in both AP and ML directions.
506 Applying N&B stability measures, the conclusions may be drawn that the normal and fast

507 walking speeds are equally stable during loading phases and a fast speed walk decrease in
508 instability during the unloading phase of double limb support.

509 A comparison between stability outcomes from neuromotor O/Is i.e. CoP-velocity and
510 CoM-oscillations illustrated that during loading phases, the outputs have more stable and less
511 unstable margins (magnitudes) compared with respective inputs during both loading and
512 unloading phases as illustrated earlier in Fig. 5. Furthermore, the gain margins quantified
513 applying N&B methods illustrated the robustness of O/I impulsive responses in terms of
514 magnitudes. During loading, all walking conditions showed infinite GMs which means
515 neuromotor control is robust enough to accommodate large perturbations while loading. This
516 was also illustrated during the respective unloading phases in which there is a significant
517 decrease in input GMs observed compared with outputs. That increase in output's stability
518 during loading and decrease in output's instability during the unloading illustrates the
519 neuromotor balance control ability in response to somatosensory inputs.

520 *4.1. Limitations*

521 Unlike in MoS evaluations, the N&B methods are appropriate for dynamic gait assessments
522 and are not suitable for a static gait. These methods are sensitive to best-fit models applying
523 system identification as a small compromise in best fit can result in a large difference in
524 stability margins. This study evaluated anterior-posterior GRFs as a somatosensory input,
525 however, the vertical GRF having maximum magnitudes are needed to be investigated in
526 future. Lastly, the walking speeds are evaluated for over ground trials which increase the
527 variance among the participants at each preferred speed. Treadmill based trials are speculated
528 to illustrate further stability differences during gait transitional phases.

529 **5. Conclusions**

530 Stability margins evaluated during gait transitional phases illustrated significant differences
531 in loading phases and partially affected unloading phases. The rotational impairments
532 significantly decreased stabilities during loading phases both in AP and ML directions and only
533 inverted foot illustrated decrease in forward instability during the unloading phase. A slow
534 speed walk showed a decrease in loading stability and a fast speed walk illustrated a decrease
535 in instability during the unloading phase of double limb support. The methods described in the
536 current manuscript also illustrate the neuromotor balance control ability quantified distinctly
537 from input and output responses. The N&B methods provide an alternative stability assessment
538 technique with the advantage of distinct criteria and evaluation of gait subphase. The use of
539 resultant neuromechanical signals makes these methods potentially suitable for stability
540 evaluation in either type of lower limb impairments, with/without wearable devices, and
541 walking on varying terrains.

542 **6. Declarations of interest:**

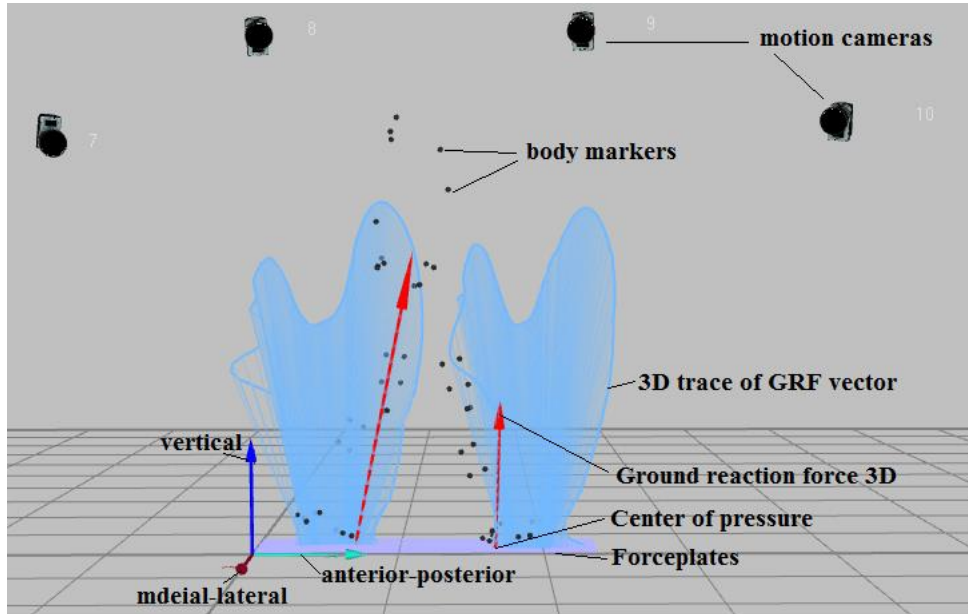
543 None.

544 **Acknowledgements**

545 The corresponding author would like to thank his PhD scholarship sponsor, University of
546 Engineering and Technology, Lahore, Pakistan. The authors would like to thank all the
547 participants and lab staff.

548 **Appendix A: Supplementary Figures and Tables**

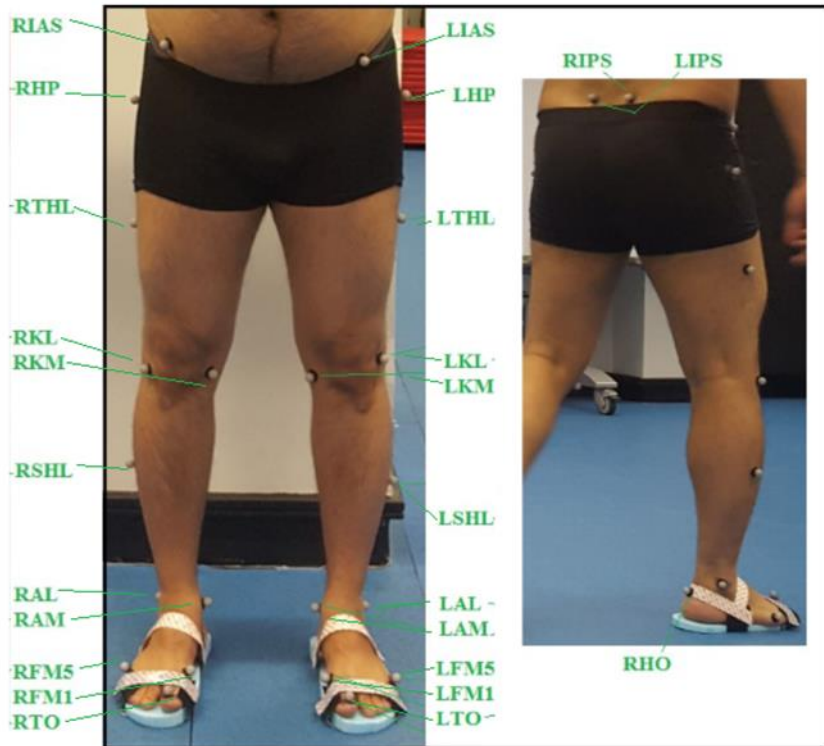
549



550

551 **Figure A.1 Motion capture system and measurement signals illustrating ground**
 552 **reaction force vector trace with tail presenting centre of pressure trajectory and vector**
 553 **head present CoM-acceleration (GRF/mass).**

554

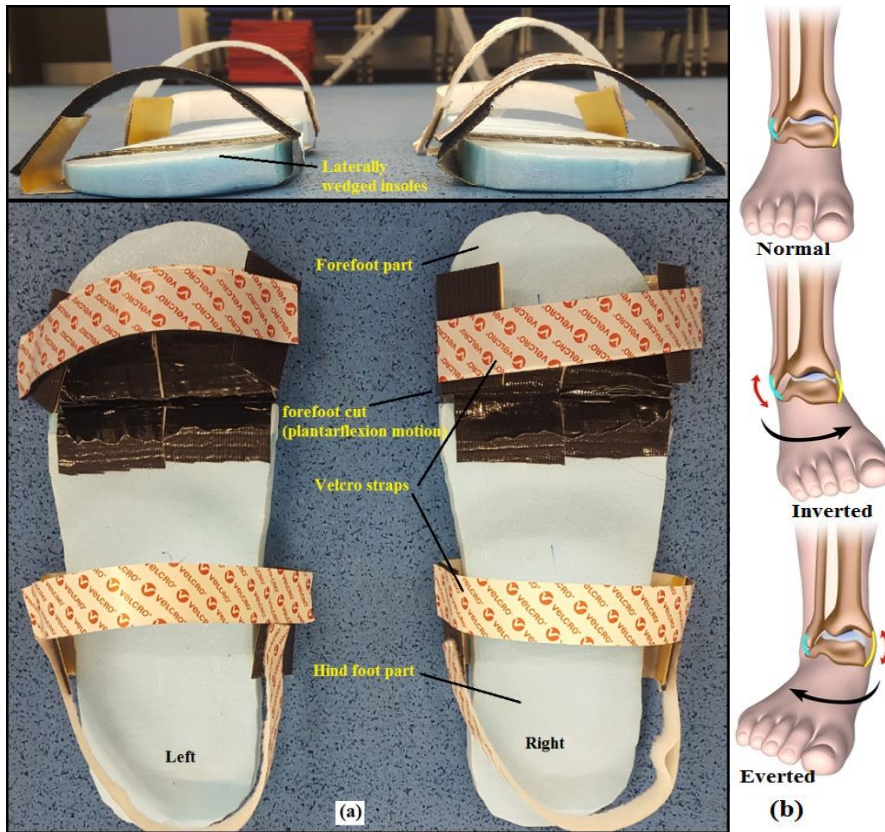


555

556 **Figure A.2 Markers placement at lower-limbs anatomical positions illustrated.**

557

558



559

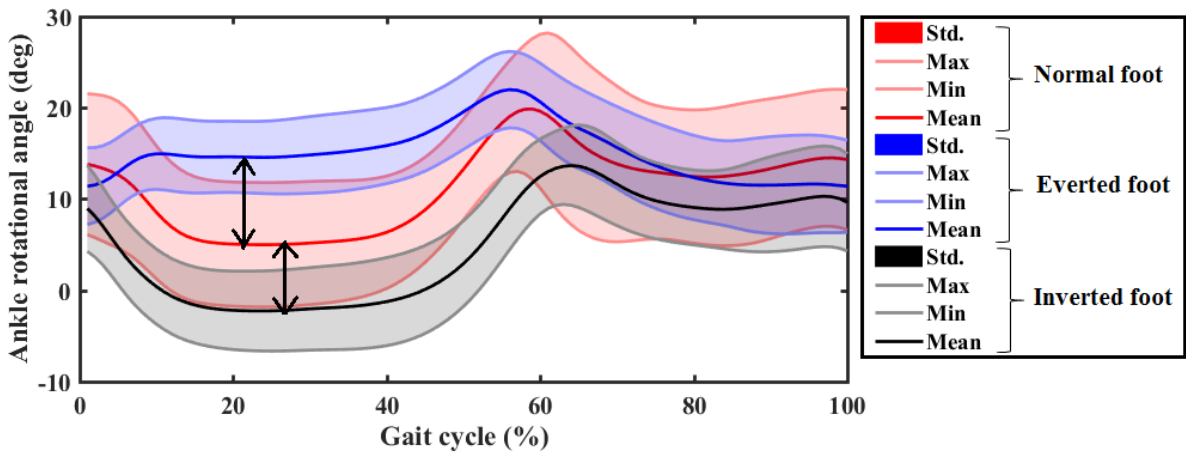
560

561

562

563

Figure A.3 (a) Wedged insoles illustrated for inverted foot walk, (b) rotational foot abnormalities illustrated, fig. adopted from <https://www.oastaug.com/ankle-sprains-high-vs-low/>.



564

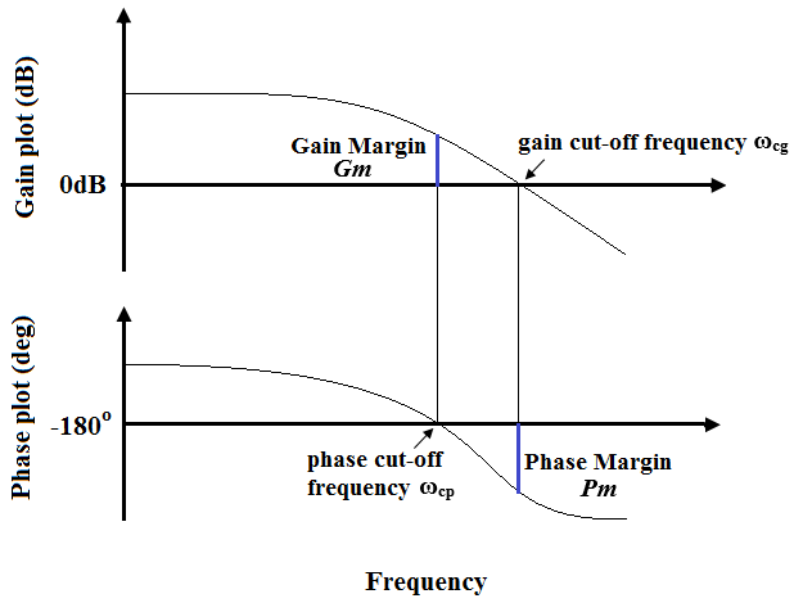
565

566

567

568

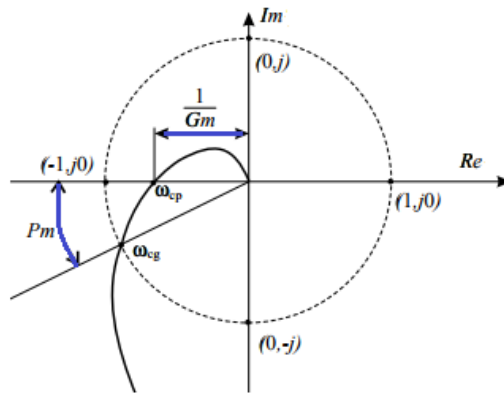
Figure A.4 Ankle-foot rotational angles illustrated for the normal and simulated inverted and everted foot conditions. A maximum difference (arrows) between the normal-everted foot and normal-inverted foot trajectories illustrate the rotational angles obtained experimentally in response to wedged foot insoles.



569

570

(a) Bode plots



571

572

(b) Nyquist plot

Figure A.5 Bode plots and equivalent Nyquist plot illustrating distinct references, cut-off frequencies and stability margins.

573

574

575

576

577

578

579

580

581

582

583

584 **Table A.1 Stability margins quantified from CoP-velocity and MoS(s) for walking speed**
 585 **and rotational impairments.**

Walking Conditions	GM (dB)	PM (deg)	MoS-HC (m)	GM (dB)	PM (deg)	MoS-TO (m)
Anterior-posterior						
Normal	∞	91.7 1.27	0.296 0.032	-15.78 3.14	80.07 3.18	0.292 0.026
Slow	∞	91.03 0.45	0.289 0.04	-15.91 2.51	80.42 3.18	0.261 0.03
Fast	∞	91.53 0.86	0.301 0.025	-10.79 4.01	71.38 8.12	0.304 0.024
Eversion	∞	90.75 0.32	0.273 0.021	-14.33 2.58	78.41 3.71	0.268 0.031
Inversion	∞	90.59 0.21	0.273 0.027	-12.58 3.21	75.46 5.61	0.270 0.023
Medial-lateral						
Normal	∞	92.28 1.45	0.0494 0.008	-12.45 2.52	75.65 3.98	0.0609 0.013
Slow	∞	91.51 0.81	0.0604 0.0132	-13.26 3.06	76.71 4.58	0.0734 0.008
Fast	∞	91.92 1.12	0.0612 0.008	-9.27 3.41	68.11 8.8	0.0747 0.013
Eversion	∞	91.14 0.40	0.0316 0.011	-11.40 3.26	73.22 6.44	0.0566 0.014
Inversion	∞	91.0 0.38	0.0606 0.013	-11.27 3.26	72.89 7.07	0.079 0.013

586 Bold values showing $p < 0.05$ when compared with a normal walk. Mean walking speeds i.e. Normal (1.132 m/s),
 587 Slow (0.86 m/s), and Fast (1.356 m/s).

588 **Table A.2 Stability margins quantified from CoM-oscillations for walking speed and**
 589 **rotational impairments.**

Walking Condition	GM (dB)	PM (deg)	GM (dB)	PM (deg)
Normal	-148.66 6.75	78.36 12.90	-111.96 2.33	89.963 0.009
Slow	-148.66 6.75	78.36 12.90	-114.72 3.75	89.917 0.023
Fast	-141.30 3.46	87.48 2.42	-114.87 2.66	89.973 0.012
Eversion	-133.11 3.91	89.37 2.27	-104.03 9.46	89.899 0.11
Inversion	-142.53 7.56	85.06 3.59	-115.37 2.16	90.101 0.308

590 Bold values showing $p < 0.05$ when compared with a normal walk.

591 Appendix B: Abbreviations

592	BoS	base of support
593	CoM	centre of mass
594	CoP	centre of pressure
595	deg	degree (unit of angle)
596	dB	decibel (unit of gain)
597	GM	gain margin
598	GRF	ground reaction force
599	I/P	input
600	LTI	linear time-invariant
601	MoS	margin of stability
602	N&B	Nyquist and Bode
603	O/I	output/input
604	O/P	output
605	PCA	principal component analysis
606	PM	phase margin
607	R ²	coefficient of determinant
608	ROM	range of motion
609	Std.	standard deviation
610	TF	transfer function
611	XCoM	extrapolated CoM

612

613

614

615

616

617

618

619

620

621

622

623

624 **References**

- 625 Allen, J. L., & Ting, L. H. (2016). Why Is Neuromechanical Modeling of Balance and Locomotion So
626 Hard? In B. I. Prilutsky & D. H. Edwards (Eds.), *Neuromechanical Modeling of Posture and*
627 *Locomotion* (pp. 197-223). New York, NY: Springer New York.
- 628 Anderson, S. R., Porrill, J., Sklavos, S., Gandhi, N. J., Sparks, D. L., & Dean, P. (2009). Dynamics of
629 Primate Oculomotor Plant Revealed by Effects of Abducens Microstimulation. *Journal of*
630 *Neurophysiology*, 101(6), 2907-2923. doi: 10.1152/jn.91045.2008
- 631 Ardestani, M. M., ZhenXian, C., Noori, H., Moazen, M., & Jin, Z. (2019). Computational Analysis of
632 Knee Joint Stability Following Total Knee Arthroplasty. *Journal of Biomechanics*. doi:
633 <https://doi.org/10.1016/j.jbiomech.2019.01.029>
- 634 Bavafa-Toosi, Y. (2017). 6 - Nyquist plot. In Y. Bavafa-Toosi (Ed.), *Introduction to Linear Control*
635 *Systems* (pp. 471-575): Academic Press.
- 636 Bekkers, E. M. J., Dockx, K., Heremans, E., Vercruyssen, S., Verschueren, S. M. P., Mirelman, A., &
637 Nieuwboer, A. (2014). The contribution of proprioceptive information to postural control in
638 elderly and patients with Parkinson's disease with a history of falls. *Frontiers in human*
639 *neuroscience*, 8, 939-939. doi: 10.3389/fnhum.2014.00939
- 640 Beyaert, C., Vasa, R., & Frykberg, G. E. (2015). Gait post-stroke: Pathophysiology and rehabilitation
641 strategies. *Neurophysiologie Clinique/Clinical Neurophysiology*, 45(4), 335-355. doi:
642 <http://dx.doi.org/10.1016/j.neucli.2015.09.005>
- 643 Bizovska, L., Svoboda, Z., Kutilek, P., Janura, M., Gaba, A., & Kovacikova, Z. (2014). Variability of
644 centre of pressure movement during gait in young and middle-aged women. *Gait & Posture*,
645 40(3), 399-402. doi: <https://doi.org/10.1016/j.gaitpost.2014.05.065>
- 646 Blum, K. P., Lamotte D'Incamps, B., Zytynicki, D., & Ting, L. H. (2017). Force encoding in muscle
647 spindles during stretch of passive muscle. *PLOS Computational Biology*, 13(9), e1005767. doi:
648 10.1371/journal.pcbi.1005767
- 649 Bruijn, S. M., van Dieën, J. H., Meijer, O. G., & Beek, P. J. (2009). Is slow walking more stable? *Journal*
650 *of Biomechanics*, 42(10), 1506-1512. doi: <https://doi.org/10.1016/j.jbiomech.2009.03.047>
- 651 C-Motion_Angles. (2019). [https://c-](https://c-motion.com/v3dwiki/index.php/Tutorial:_Foot_and_Ankle_Angles)
652 [motion.com/v3dwiki/index.php/Tutorial:_Foot_and_Ankle_Angles](https://c-motion.com/v3dwiki/index.php/Tutorial:_Foot_and_Ankle_Angles)
- 653 C-Motion_Markers. (2019). [https://www.c-](https://www.c-motion.com/v3dwiki/index.php/Marker_Set_Guidelines#Model_1)
654 [motion.com/v3dwiki/index.php/Marker_Set_Guidelines#Model_1](https://www.c-motion.com/v3dwiki/index.php/Marker_Set_Guidelines#Model_1).
- 655 Cattaneo, D., Rabuffetti, M., Bovi, G., Mevio, E., Jonsdottir, J., & Ferrarin, M. (2014). Assessment of
656 postural stabilization in three task oriented movements in people with multiple sclerosis.
657 *Disability and Rehabilitation*, 36(26), 2237-2243. doi: 10.3109/09638288.2014.904933
- 658 Cohen, M. X. (2014). *Analyzing neural time series data: theory and practice - Chapter 23*: MIT press.
- 659 DiDomenico, A., McGorry, R. W., & Banks, J. J. (2013). Methodological considerations of existing
660 techniques for determining stabilization times following a multi-planar transition. *Gait &*
661 *Posture*, 38(3), 541-543. doi: <http://dx.doi.org/10.1016/j.gaitpost.2013.01.011>
- 662 Downes, T. P., Welch, D., Scott, K. S., Austermann, J., Wilson, G. W., & Yun, M. S. (2012). Calculating
663 the transfer function of noise removal by principal component analysis and application to
664 AzTEC deep-field observations. *Monthly Notices of the Royal Astronomical Society*, 423(1),
665 529-542. doi: 10.1111/j.1365-2966.2012.20896.x
- 666 Fan, Y., Li, Z., Han, S., Lv, C., & Zhang, B. (2016). The influence of gait speed on the stability of walking
667 among the elderly. *Gait & Posture*, 47, 31-36. doi:
668 <https://doi.org/10.1016/j.gaitpost.2016.02.018>
- 669 Gigi, R., Haim, A., Luger, E., Segal, G., Melamed, E., Beer, Y., . . . Elbaz, A. (2015). Deviations in gait
670 metrics in patients with chronic ankle instability: a case control study. *Journal of Foot and*
671 *Ankle Research*, 8(1), 1. doi: 10.1186/s13047-014-0058-1
- 672 Graham, D. F., Carty, C. P., Lloyd, D. G., & Barrett, R. S. (2017). Muscle contributions to the
673 acceleration of the whole body centre of mass during recovery from forward loss of balance

- 674 by stepping in young and older adults. *PLOS ONE*, 12(10), e0185564. doi:
 675 10.1371/journal.pone.0185564
- 676 Hernández, A., Silder, A., Heiderscheit, B. C., & Thelen, D. G. (2009). Effect of age on center of mass
 677 motion during human walking. *Gait & Posture*, 30(2), 217-222. doi:
 678 <https://doi.org/10.1016/j.gaitpost.2009.05.006>
- 679 Hof, A. L. (2008). The 'extrapolated center of mass' concept suggests a simple control of balance in
 680 walking. *Human Movement Science*, 27(1), 112-125. doi:
 681 <https://doi.org/10.1016/j.humov.2007.08.003>
- 682 Hur, P., Duiser, B. A., Salapaka, S. M., & Hsiao-Wecksler, E. T. (2010). Measuring Robustness of the
 683 Postural Control System to a Mild Impulsive Perturbation. *IEEE Transactions on Neural
 684 Systems and Rehabilitation Engineering*, 18(4), 461-467. doi: 10.1109/TNSRE.2010.2052133
- 685 Ihlen, E. A. F., Goihl, T., Wik, P. B., Sletvold, O., Helbostad, J., & Vereijken, B. (2012). Phase-
 686 dependent changes in local dynamic stability of human gait. *Journal of Biomechanics*, 45(13),
 687 2208-2214. doi: <https://doi.org/10.1016/j.jbiomech.2012.06.022>
- 688 ImageJ-macros. (2019). [http://dev.mri.cnrs.fr/projects/imagej-
 689 macros/wiki/Velocity_Measurement_Tool](http://dev.mri.cnrs.fr/projects/imagej-macros/wiki/Velocity_Measurement_Tool)
- 690 Inspect3D. (2018). https://www.c-motion.com/v3dwiki/index.php/Inspect3D_Overview. 2018.
- 691 Kang, H. G., & Dingwell, J. B. (2009). Dynamics and stability of muscle activations during walking in
 692 healthy young and older adults. *Journal of Biomechanics*, 42(14), 2231-2237. doi:
 693 <https://doi.org/10.1016/j.jbiomech.2009.06.038>
- 694 Kavanagh, J. J. (2009). Lower trunk motion and speed-dependence during walking. [journal article].
 695 *Journal of NeuroEngineering and Rehabilitation*, 6(1), 9. doi: 10.1186/1743-0003-6-9
- 696 La Scaleia, V., Ivanenko, Y. P., Zelik, K. E., & Lacquaniti, F. (2014). Spinal motor outputs during step-
 697 to-step transitions of diverse human gaits. *Frontiers in Human Neuroscience*, 8, 305. doi:
 698 10.3389/fnhum.2014.00305
- 699 Lencioni, T., Rabuffetti, M., Piscoquito, G., Pareyson, D., Aiello, A., Di Sipio, E., . . . Ferrarin, M.
 700 (2014). Postural stabilization and balance assessment in Charcot–Marie–Tooth 1A subjects.
 701 *Gait & Posture*, 40(4), 481-486. doi: <https://doi.org/10.1016/j.gaitpost.2014.07.006>
- 702 Lu, H.-L., Kuo, M.-Y., Chang, C.-F., Lu, T.-W., & Hong, S.-W. (2017). Effects of gait speed on the body's
 703 center of mass motion relative to the center of pressure during over-ground walking. *Human
 704 Movement Science*, 54, 354-362. doi: <https://doi.org/10.1016/j.humov.2017.06.004>
- 705 Lu, H.-L., Lu, T.-W., Lin, H.-C., Hsieh, H.-J., & Chan, W. P. (2017). Effects of belt speed on the body's
 706 center of mass motion relative to the center of pressure during treadmill walking. *Gait &
 707 Posture*, 51, 109-115. doi: <https://doi.org/10.1016/j.gaitpost.2016.09.030>
- 708 Lugade, V., & Kaufman, K. (2014). Center of pressure trajectory during gait: A comparison of four
 709 foot positions. *Gait & Posture*, 40(4), 719-722. doi:
 710 <http://dx.doi.org/10.1016/j.gaitpost.2014.07.001>
- 711 Lugade, V., Lin, V., & Chou, L.-S. (2011). Center of mass and base of support interaction during gait.
 712 *Gait & posture*, 33(3), 406-411.
- 713 Maslivec, A., Bampouras, T. M., Dewhurst, S., Vannozzi, G., Macaluso, A., & Laudani, L. (2018).
 714 Mechanisms of head stability during gait initiation in young and older women: A neuro-
 715 mechanical analysis. *Journal of Electromyography and Kinesiology*, 38, 103-110. doi:
 716 <https://doi.org/10.1016/j.jelekin.2017.11.010>
- 717 Mei, Z., Zhao, G., Ivanov, K., Guo, Y., Zhu, Q., Zhou, Y., & Wang, L. (2013). Sample entropy
 718 characteristics of movement for four foot types based on plantar centre of pressure during
 719 stance phase. [journal article]. *BioMedical Engineering OnLine*, 12(1), 101. doi:
 720 10.1186/1475-925x-12-101
- 721 Morgan, K. D., Zheng, Y., Bush, H., & Noehren, B. (2016). Nyquist and Bode stability criteria to assess
 722 changes in dynamic knee stability in healthy and anterior cruciate ligament reconstructed
 723 individuals during walking. *Journal of Biomechanics*, 49(9), 1686-1691. doi:
 724 <http://dx.doi.org/10.1016/j.jbiomech.2016.03.049>

- 725 Neptune, R., & Vistamehr, A. (2018). Dynamic Balance during Human Movement: Measurement and
726 Control Mechanisms. *Journal of Biomechanical Engineering*. doi: 10.1115/1.4042170
- 727 Öunpuu, S., Garibay, E., Solomito, M., Bell, K., Pierz, K., Thomson, J., . . . DeLuca, P. (2013). A
728 comprehensive evaluation of the variation in ankle function during gait in children and youth
729 with Charcot–Marie–Tooth disease. *Gait & Posture*, *38*(4), 900-906. doi:
730 <https://doi.org/10.1016/j.gaitpost.2013.04.016>
- 731 Portela, F. M., Rodrigues, E. C., & de Sá Ferreira, A. (2014). A critical review of position-and velocity-
732 based concepts of postural control during upright stance. *Human Movement*, *15*(4), 227-233.
- 733 Rabiej, M., Eslami, M., & Movaghar, A. F. (2016). The assessment of three-dimensional foot
734 pronation using a principal component analysis method in the stance phase of running. *The*
735 *Foot*, *29*, 11-17. doi: <https://doi.org/10.1016/j.foot.2016.09.008>
- 736 Rabuffetti, M., Bovi, G., Quadri, P. L., Cattaneo, D., Benvenuti, F., & Ferrarin, M. (2011). An
737 experimental paradigm to assess postural stabilization: no more movement and not yet
738 posture. *IEEE Transactions on Neural Systems and Rehabilitation Engineering*, *19*(4), 420-
739 426.
- 740 Robbins, S. M., Astephen Wilson, J. L., Rutherford, D. J., & Hubble-Kozey, C. L. (2013). Reliability of
741 principal components and discrete parameters of knee angle and moment gait waveforms in
742 individuals with moderate knee osteoarthritis. *Gait & Posture*, *38*(3), 421-427. doi:
743 <https://doi.org/10.1016/j.gaitpost.2013.01.001>
- 744 Sivakumaran, S., Schinkel-Ivy, A., Masani, K., & Mansfield, A. (2018). Relationship between margin of
745 stability and deviations in spatiotemporal gait features in healthy young adults. *Human*
746 *Movement Science*, *57*, 366-373. doi: <https://doi.org/10.1016/j.humov.2017.09.014>
- 747 Sklavos, S., Porrill, J., Kaneko, C. R. S., & Dean, P. (2005). Evidence for wide range of time scales in
748 oculomotor plant dynamics: Implications for models of eye-movement control. *Vision*
749 *Research*, *45*(12), 1525-1542. doi: <https://doi.org/10.1016/j.visres.2005.01.005>
- 750 Soares, D. P., de Castro, M. P., Mendes, E., & Machado, L. (2014). Influence of wedges on lower
751 limbs' kinematics and net joint moments during healthy elderly gait using principal
752 component analysis. *Human Movement Science*, *38*, 319-330. doi:
753 <https://doi.org/10.1016/j.humov.2014.09.007>
- 754 Svoboda, Z., Bizovska, L., Janura, M., Kubonova, E., Janurova, K., & Vuillerme, N. (2017). Variability of
755 spatial temporal gait parameters and center of pressure displacements during gait in elderly
756 fallers and nonfallers: A 6-month prospective study. *PLOS ONE*, *12*(2), e0171997. doi:
757 [10.1371/journal.pone.0171997](https://doi.org/10.1371/journal.pone.0171997)
- 758 Tan, M. H., & Hammond, J. K. (2007). A non-parametric approach for linear system identification
759 using principal component analysis. *Mechanical Systems and Signal Processing*, *21*(4), 1576-
760 1600. doi: <https://doi.org/10.1016/j.ymsp.2006.07.005>
- 761 van der Linden, M. H., van der Linden, S. C., Hendricks, H. T., van Engelen, B. G. M., & Geurts, A. C. H.
762 (2010). Postural instability in Charcot-Marie-Tooth type 1A patients is strongly associated
763 with reduced somatosensation. *Gait & Posture*, *31*(4), 483-488. doi:
764 <https://doi.org/10.1016/j.gaitpost.2010.02.005>
- 765 Winter, D. A. (2009). *Biomechanics and motor control of human movement*: John Wiley & Sons.

766

767

768